

基于 PINNs 的压电半导体梁的非线性多场耦合力学分析*

肖争光¹, 张春利^{1,2}, 陈伟球^{1,2}

(1. 浙江大学 航空航天学院, 杭州 310027;

2. 浣江实验室, 浙江 诸暨 311816)

(我刊青年编委张春利、编委陈伟球来稿)

摘要: 压电半导体(PS)具有压电性和半导体特性共存耦合的特征,在新型多功能电子/光电子学器件中有广阔应用前景.因此,理论分析压电半导体结构在外载作用下的多场耦合力学响应是十分重要的.然而,描述压电半导体多场耦合力学行为的控制方程中含有非线性的电流方程,属于物理非线性;而且很多半导体器件通常工作在大变形模式下,在力学上属于几何非线性问题.物理非线性和几何非线性给问题的求解带来了挑战.该文针对压电半导体梁结构,基于物理信息神经网络(physics informed neural networks, PINNs),构建了能高效求解其非线性多场耦合力学问题的 PINNs 方法.通过依次删除网络结构中载流子项和压电项,该方法即可退化到压电结构和纯弹性结构的情况.利用所构建的 PINNs,分析了压电半导体梁在均布压力下的多场耦合力学响应.数值结果表明:该文所提出的基于 PINNs 的模型能有效求解压电半导体、压电以及纯弹性结构非线性多场耦合问题,相对而言,其在求解压电和纯弹性结构的力学响应时具有更高的精度.

关键词: 压电半导体梁; 多场耦合; 非线性; PINNs

中图分类号: O343.5 **文献标志码:** A **DOI:** 10.21656/1000-0887.450070

Analysis of Nonlinear Multi-Field Coupling Mechanics of Piezoelectric Semiconductor Beams via PINNs

XIAO Zhengguang¹, ZHANG Chunli^{1,2}, CHEN Weiqiu^{1,2}

(1. School of Aeronautics and Astronautics, Zhejiang University, Hangzhou 310027, P.R.China;

2. Huanjiang Laboratory, Zhuji, Zhejiang 311816, P.R.China)

(Contributed by ZHANG Chunli, M.AMM Youth Editorial Board & CHEN Weiqiu, M.AMM Editorial Board)

Abstract: Piezoelectric semiconductors (PSs) possess the characteristics of coexistence of piezoelectric and semiconductor properties and have broad application prospects in new multifunctional electronic/optoelectronic

* 收稿日期: 2024-03-19; 修订日期: 2024-04-26

基金项目: 国家自然科学基金(面上项目)(12172326;11972319);国家重点研发计划(2020YFA0711701; 2020YFA0711700)

作者简介: 肖争光(1995—),男,博士生(E-mail: 12124091@zju.edu.cn);

张春利(1980—),男,教授,博士,博士生导师(通讯作者. E-mail: zhangcl01@zju.edu.cn);

陈伟球(1969—),男,教授,博士,博士生导师,教育部长江学者特聘教授(E-mail: chenwq@zju.edu.cn).

引用格式: 肖争光,张春利,陈伟球.基于 PINNs 的压电半导体梁的非线性多场耦合力学分析[J].应用数学和力学,2024,45(10):1288-1299.

devices. It is very important to theoretically analyze multi-field coupling mechanical responses of PS structures under external loads. However, the governing equations describing the multi-field coupling mechanical behaviors of PS structures contain physically nonlinear current equations. On the other hand, many semiconductor devices typically operate under large deformation, which raises a geometrically nonlinear problem. The presence of physical and geometric nonlinearity poses challenges to the solution of the problem. Herein, for PS beam structures, a method based on physics informed neural networks (PINNs) was established to efficiently solve their nonlinear multi-field coupling responses. Through successive elimination of carrier-related terms and piezoelectricity-related terms from the constructed PINNs, the proposed method can be reduced to the cases of piezoelectric and pure elastic structures, respectively. With the proposed PINNs, the multi-field coupling responses of a PS beam under static uniform pressure were predicted. Numerical results show that, the proposed method can effectively solve the nonlinear multi-field coupling problems of the PS, piezoelectric and pure elastic structures. Relatively, it exhibits higher accuracy in solving piezoelectric and pure elastic structures.

Key words: PS beam; multi-field coupling; nonlinearity; PINNs

0 引 言

压电半导体因具有压电特性和半导体特性,而被广泛应用在多功能电子元器件领域,例如:超声放大器、晶体管、滤波器和能量采集器等^[1-5]。目前,基于唯象学的压电半导体理论研究,大多是对压电半导体基本方程进行线性化假设,例如通过漂移电流的线性化假设来忽略其中的非线性项而进行理论研究,这包括:压电半导体结构多场耦合力学行为分析^[6]、磁场作用下的压电半导体圆柱壳耦合响应分析^[7]、多温度载荷下压电半导体的压电电子学行为分析^[8],以及弹性波在压电半导体杆中的传播^[9]等。特别地,基于漂移电流的线性化假设,Zhang 等^[10]和王晓媛^[11]从压电半导体的三维基本方程出发,导出了拉伸变形模式下的一维基本方程,并获得了两端自由的压电半导体杆在自平衡状态下的位移、电场和载流子的分布情况。Cheng 等^[12]和 Luo 等^[13]研究发现,压电效应、热释电和热弹性效应的相互作用能够实现温度场对压电-半导体复合结构中载流子的分布调控。类似地,Zhang 等^[14]还得到了氧化锌纳米杆在受轴向拉伸时杆内各物理场的解析解。Fan 等^[15]研究了氧化锌纳米杆在受局部轴向应力时各物理场的解析解,并发现应力场可用于调控氧化锌纳米杆中的电学行为。为探索氧化锌纳米线的器件应用,Huang 等^[16]分析了局部拉/压应力对氧化锌杆电流-电压曲线的影响。这些研究对压电半导体器件的设计与应用具有一定的指导意义。

目前,学者们虽利用线性化方法对压电半导体多场耦合力学问题开展了许多理论分析,也取得了一些有益的结果,但是,线性化分析方法只适用于载荷较小的情况,不能准确求解较大载荷的情况。为此,一些学者考虑载流子的非线性漂移-扩散模型,研究了压电半导体结构在外载下的多场耦合力学响应。例如,Ancona 等^[17-20]考虑大变形导出了相应的三维非线性方程,并数值求解了 III-V 族半导体器件结构热-电-弹耦合力学问题。最近,郑州大学赵明峰教授团队采用迭代法^[21]、同伦分析法^[22]和打靶法^[23]等数值方法,研究了压电半导体纤维在局部拉伸/压缩应力和电场作用下的电响应。上述研究主要集中在物理非线性上,即载流子漂移电流的非线性,而没有考虑几何非线性。最近,Bao 等^[24]考虑几何非线性,采用摄动法导出了压电半导体杆轴向变形的解析解。截止目前,针对压电半导体结构,同时考虑几何和物理非线性的研究还很少,亟需发展相应的非线性全耦合力学问题的高效分析方法。

机器学习(ML)是当前科技的研究热点,特别是在人工智能及模式识别领域,已被广泛应用于解决各学科领域复杂问题的求解,例如:数学^[25-27]、材料科学^[28-29]、力学^[30]、生物医学^[31]等领域。Raissi 等^[32]在神经网络损失函数中引入了能描述物理定律的项,构建了融合物理信息的神经网络结构(PINNs)。PINNs 通过将物理原理整合到训练过程中,从而捕获潜在的物理原理,并提高了预测的准确性和可靠性。PINNs 克服了常用的深度、卷积和循环神经网络的主要缺点(即鲁棒性和收敛性难以保证),为求解非线性偏微分方程提供了一种有效的方法。为了使 PINNs 能够求解任意复杂几何域上的非线性偏微分方程,Jagtap 等^[33]提出了一种广义时空域分解框架。PINNs 为解决不同科学领域的复杂非线性问题带来了新的思路。我们知道:力学各分支学

科(如流体力学和固体力学)领域也涉及大量由非线性偏微分方程控制的多物理场耦合问题,而传统的处理手段大都不能很好地解决这类非线性多场耦合问题.同样,PINNs技术为此类复杂力学问题的分析与预测提供了新思路.例如,Raissi等^[34]将 Navier-Stokes 方程编码到 PINNs 中,来描述流体的流动模式,且不受几何或初始条件和边界条件的影响;Haghighat等^[35]采用 PINNs 研究了固体力学中的反演问题等.

本文将 PINNs 拓展到求解压电半导体结构在外载下的非线性多场耦合力学分析中.首先,考虑广义平面应变问题,给出了压电半导体梁的基本控制方程,包括运动平衡方程,电学 Gauss 方程,电荷连续性方程,应力、电位移和电流的本构方程,以及非线性应变-位移关系、电场-电势关系.其次,在上述基本方程的基础上,构建了适用于压电半导体梁结构非线性多场耦合力学行为分析的 PINNs 模型.然后,采用所构建的 PINNs 模型分析了压电半导体梁在均布载荷作用下的静力学响应.通过把 PINNs 模型退化到压电梁和弹性梁的情况,利用压电梁和弹性梁有限元计算结果,理论验证了所构建的 PINNs 的正确性和可靠性.

1 压电半导体梁非线性模型

考虑如图 1 所示的 n 型压电半导体梁,其轴向沿 x 方向,厚度沿 z 方向.为分析问题方便,考虑广义平面应变问题,即所有物理量均与 y 方向无关.根据压电半导体三维方程^[6],可写出不考虑体力时的压电半导体梁的运动平衡方程、电学 Gauss 方程和电荷连续性方程:

$$\begin{cases} \frac{\partial T_{xx}}{\partial x} + \frac{\partial T_{xz}}{\partial z} = \rho \ddot{u}, \\ \frac{\partial T_{xz}}{\partial x} + \frac{\partial T_{zz}}{\partial z} = \rho \ddot{w}, \\ \frac{\partial D_x}{\partial x} + \frac{\partial D_z}{\partial z} = q(-n + N_D^+), \\ \frac{\partial J_x}{\partial x} + \frac{\partial J_z}{\partial z} = q \dot{n}, \end{cases} \quad (1)$$

其中 T_{xx}, T_{xz}, T_{zz} 为应力分量, D_x, D_z 为电位移分量, J_x, J_z 为电子电流密度分量, ρ 为质量密度, u 和 w 分别为 x 和 z 方向位移, n 为电子浓度, N_D^+ 为半导体掺杂总的施主浓度, q 为基本电荷量 (1.602×10^{-19} C).

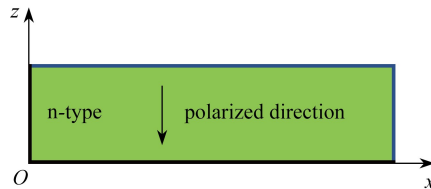


图 1 压电半导体梁的示意图

Fig. 1 The sketch of a piezoelectric semiconductor beam

n 型压电半导体的本构方程为

$$\begin{cases} \begin{Bmatrix} T_{xx} \\ T_{zz} \\ T_{xz} \end{Bmatrix} = \begin{bmatrix} c_{11} & c_{13} & 0 \\ c_{13} & c_{33} & 0 \\ 0 & 0 & c_{55} \end{bmatrix} \begin{Bmatrix} S_{xx} \\ S_{zz} \\ S_{xz} \end{Bmatrix} - \begin{bmatrix} 0 & e_{31} \\ 0 & e_{33} \\ e_{15} & 0 \end{bmatrix} \begin{Bmatrix} E_x \\ E_z \end{Bmatrix}, \\ \begin{Bmatrix} D_x \\ D_z \end{Bmatrix} = \begin{bmatrix} 0 & 0 & e_{15} \\ e_{31} & e_{33} & 0 \end{bmatrix} \begin{Bmatrix} S_{xx} \\ S_{zz} \\ S_{xz} \end{Bmatrix} + \begin{bmatrix} \varepsilon_{11} & 0 \\ 0 & \varepsilon_{33} \end{bmatrix} \begin{Bmatrix} E_x \\ E_z \end{Bmatrix}, \\ \begin{Bmatrix} J_x \\ J_z \end{Bmatrix} = -qn \begin{bmatrix} \mu_{11} & 0 \\ 0 & \mu_{33} \end{bmatrix} \begin{Bmatrix} \varphi_{,x} \\ \varphi_{,z} \end{Bmatrix} + q \begin{bmatrix} D_{11} & 0 \\ 0 & D_{33} \end{bmatrix} \begin{Bmatrix} n_x \\ n_z \end{Bmatrix}, \end{cases} \quad (2)$$

其中 $c_{11}, c_{13}, c_{33}, c_{55}$ 为弹性常数, S_{xx}, S_{xz}, S_{zz} 为应变分量, E_x, E_z 为电场分量, φ 为电势, e_{31}, e_{33}, e_{15} 为压电常数, $\varepsilon_{11}, \varepsilon_{33}$ 为介电常数, μ_{11}, μ_{33} 为电子迁移率, D_{11}, D_{33} 为电子扩散常数.

Von Kármán 非线性应变-位移关系为^[36]

$$\begin{cases} S_{xx} = \frac{\partial u}{\partial x} + \frac{1}{2} \left(\frac{\partial w}{\partial x} \right)^2, \\ S_{zz} = \frac{\partial w}{\partial z}, \\ S_{xz} = \frac{\partial u}{\partial z} + \frac{\partial w}{\partial x}. \end{cases} \quad (3)$$

电场和电子浓度梯度为

$$\begin{cases} E_x = -\frac{\partial \varphi}{\partial x}, E_z = -\frac{\partial \varphi}{\partial z}, \\ n_x = \frac{\partial n}{\partial x}, n_z = \frac{\partial n}{\partial z}. \end{cases} \quad (4)$$

将式(2)–(4)代入式(1)中,可得

$$\begin{cases} c_{11}u_{,xx} + c_{11}w_{,x}w_{,xx} + c_{13}w_{,zx} + e_{31}\varphi_{,zx} + c_{55}u_{,zz} + c_{55}w_{,xz} + e_{15}\varphi_{,xz} = \rho\ddot{u}, \\ c_{55}u_{,zx} + c_{55}w_{,xx} + e_{15}\varphi_{,xx} + c_{13}u_{,xz} + c_{13}w_{,x}w_{,xz} + c_{33}w_{,zz} + e_{33}\varphi_{,zz} = \rho\ddot{w}, \\ e_{15}u_{,zx} + e_{15}w_{,xx} - \varepsilon_{11}\varphi_{,xx} + e_{31}u_{,xz} + e_{31}w_{,x}w_{,xz} + e_{33}w_{,zz} - \varepsilon_{33}\varphi_{,zz} = q(-n + N_D^+), \\ -q\mu_{11}n_{,x}\varphi_{,x} - q\mu_{11}n\varphi_{,xx} + qD_{11}n_{,xx} - q\mu_{33}n_{,z}\varphi_{,z} - q\mu_{33}n\varphi_{,zz} + qD_{33}n_{,zz} = q\dot{n}. \end{cases} \quad (5)$$

对于静力学问题,通过删去式(5)中与时间有关的项,可得

$$\begin{cases} c_{11}u_{,xx} + c_{11}w_{,x}w_{,xx} + c_{13}w_{,zx} + e_{31}\varphi_{,zx} + c_{55}u_{,zz} + c_{55}w_{,xz} + e_{15}\varphi_{,xz} = 0, \\ c_{55}u_{,zx} + c_{55}w_{,xx} + e_{15}\varphi_{,xx} + c_{13}u_{,xz} + c_{13}w_{,x}w_{,xz} + c_{33}w_{,zz} + e_{33}\varphi_{,zz} = 0, \\ e_{15}u_{,zx} + e_{15}w_{,xx} - \varepsilon_{11}\varphi_{,xx} + e_{31}u_{,xz} + e_{31}w_{,x}w_{,xz} + e_{33}w_{,zz} - \varepsilon_{33}\varphi_{,zz} - q(-n + N_D^+) = 0, \\ -q\mu_{11}n_{,x}\varphi_{,x} - q\mu_{11}n\varphi_{,xx} + qD_{11}n_{,xx} - q\mu_{33}n_{,z}\varphi_{,z} - q\mu_{33}n\varphi_{,zz} + qD_{33}n_{,zz} = 0. \end{cases} \quad (6)$$

通过引入 $\mathbf{u}(x, z) = [u(x, z), w(x, z), \varphi(x, z), n(x, z)]^T$, 可把式(6)写成矩阵形式,即

$$\mathbf{K}_1\mathbf{u}_1 + \mathbf{K}_2\mathbf{u}_2 + \mathbf{K}_3\mathbf{u}_3 + \mathbf{K}_4\mathbf{u}_4 + \mathbf{K}_5\mathbf{u}_5 + \mathbf{K}_6(\mathbf{u}_6 + \mathbf{u}_8) + \mathbf{K}_7(\mathbf{u}_7 + \mathbf{u}_9) + \mathbf{K}_8\mathbf{u}_{10} - \mathbf{q} = \mathbf{0}, \quad (7)$$

其中

$$\begin{cases} \mathbf{u}_1 = \begin{Bmatrix} u_{,xx} \\ w_{,xx} \\ \varphi_{,xx} \\ n_{,xx} \end{Bmatrix}, \mathbf{u}_2 = \begin{Bmatrix} u_{,zz} \\ w_{,zz} \\ \varphi_{,zz} \\ n_{,zz} \end{Bmatrix}, \mathbf{u}_3 = \begin{Bmatrix} u_{,xz} \\ w_{,xz} \\ \varphi_{,xz} \\ n_{,xz} \end{Bmatrix}, \mathbf{u}_4 = \begin{Bmatrix} 0 \\ w_{,x}w_{,xx} \\ 0 \\ 0 \end{Bmatrix}, \mathbf{u}_5 = \begin{Bmatrix} 0 \\ w_{,x}w_{,xz} \\ 0 \\ 0 \end{Bmatrix}, \\ \mathbf{u}_6 = \begin{Bmatrix} 0 \\ 0 \\ 0 \\ n_{,x}\varphi_{,x} \end{Bmatrix}, \mathbf{u}_7 = \begin{Bmatrix} 0 \\ 0 \\ 0 \\ n_{,z}\varphi_{,z} \end{Bmatrix}, \mathbf{u}_8 = \begin{Bmatrix} 0 \\ 0 \\ 0 \\ n\varphi_{,xx} \end{Bmatrix}, \\ \mathbf{u}_9 = \begin{Bmatrix} 0 \\ 0 \\ 0 \\ n\varphi_{,zz} \end{Bmatrix}, \mathbf{u}_{10} = \begin{Bmatrix} u \\ w \\ \varphi \\ n \end{Bmatrix}, \mathbf{q} = \begin{Bmatrix} 0 \\ 0 \\ -qN_D^+ \\ 0 \end{Bmatrix}, \end{cases} \quad (8)$$

$$\left\{ \begin{array}{l}
\mathbf{K}_1 = \begin{bmatrix} c_{11} & 0 & 0 & 0 \\ 0 & c_{55} & e_{15} & 0 \\ 0 & e_{15} & -\varepsilon_{11} & 0 \\ 0 & 0 & 0 & qD_{11} \end{bmatrix}, \mathbf{K}_2 = \begin{bmatrix} c_{55} & 0 & 0 & 0 \\ 0 & c_{33} & e_{33} & 0 \\ 0 & e_{33} & -\varepsilon_{33} & 0 \\ 0 & 0 & 0 & qD_{33} \end{bmatrix}, \\
\mathbf{K}_3 = \begin{bmatrix} 0 & c_{13} + c_{55} & e_{31} + e_{15} & 0 \\ c_{55} + c_{13} & 0 & 0 & 0 \\ e_{15} + e_{31} & 0 & 0 & 0 \\ 0 & 0 & 0 & 0 \end{bmatrix}, \mathbf{K}_4 = \begin{bmatrix} 0 & c_{11} & 0 & 0 \\ 0 & 0 & 0 & 0 \\ 0 & 0 & 0 & 0 \\ 0 & 0 & 0 & 0 \end{bmatrix}, \\
\mathbf{K}_5 = \begin{bmatrix} 0 & 0 & 0 & 0 \\ 0 & c_{13} & 0 & 0 \\ 0 & e_{31} & 0 & 0 \\ 0 & 0 & 0 & 0 \end{bmatrix}, \mathbf{K}_6 = \begin{bmatrix} 0 & 0 & 0 & 0 \\ 0 & 0 & 0 & 0 \\ 0 & 0 & 0 & 0 \\ 0 & 0 & 0 & -q\mu_{11} \end{bmatrix}, \\
\mathbf{K}_7 = \begin{bmatrix} 0 & 0 & 0 & 0 \\ 0 & 0 & 0 & 0 \\ 0 & 0 & 0 & 0 \\ 0 & 0 & 0 & -q\mu_{33} \end{bmatrix}, \mathbf{K}_8 = \begin{bmatrix} 0 & 0 & 0 & 0 \\ 0 & 0 & 0 & 0 \\ 0 & 0 & 0 & q \\ 0 & 0 & 0 & 0 \end{bmatrix}.
\end{array} \right. \quad (9)$$

2 压电半导体梁结构的 PINNs 模型

采用经典 PINNs 思想,一般形式的偏微分方程为

$$u_t + N[u; \lambda] = 0, \quad x \in \Omega, t \in [0, T], \quad (10)$$

其中 $N[u; \lambda]$ 是非线性微分算子, λ 为未知参数. 由此, 我们可把式(7)写为

$$\begin{aligned}
& N_1 \mathbf{u}_1 + N_2 \mathbf{u}_2 + N_3 \mathbf{u}_3 + N_4 \mathbf{u}_4 + N_5 \mathbf{u}_5 + \\
& N_6(\mathbf{u}_6 + \mathbf{u}_8) + N_7(\mathbf{u}_7 + \mathbf{u}_9) + N_8 \mathbf{u}_{10} - \mathbf{q} = \mathbf{0},
\end{aligned} \quad (11)$$

其中

$$\left\{ \begin{array}{l}
\mathbf{N}_1 = \begin{bmatrix} \lambda_1 & 0 & 0 & 0 \\ 0 & \lambda_4 & \lambda_5 & 0 \\ 0 & \lambda_5 & -\lambda_8 & 0 \\ 0 & 0 & 0 & \lambda_{11} \end{bmatrix}, \mathbf{N}_2 = \begin{bmatrix} \lambda_4 & 0 & 0 & 0 \\ 0 & \lambda_3 & \lambda_7 & 0 \\ 0 & \lambda_7 & -\lambda_9 & 0 \\ 0 & 0 & 0 & \lambda_{11} \end{bmatrix}, \\
\mathbf{N}_3 = \begin{bmatrix} 0 & \lambda_{13} + \lambda_4 & \lambda_6 + \lambda_5 & 0 \\ \lambda_4 + \lambda_2 & 0 & 0 & 0 \\ \lambda_5 + \lambda_6 & 0 & 0 & 0 \\ 0 & 0 & 0 & 0 \end{bmatrix}, \mathbf{N}_4 = \begin{bmatrix} 0 & \lambda_1 & 0 & 0 \\ 0 & 0 & 0 & 0 \\ 0 & 0 & 0 & 0 \\ 0 & 0 & 0 & 0 \end{bmatrix}, \mathbf{N}_5 = \begin{bmatrix} 0 & 0 & 0 & 0 \\ 0 & \lambda_2 & 0 & 0 \\ 0 & \lambda_6 & 0 & 0 \\ 0 & 0 & 0 & 0 \end{bmatrix}, \\
\mathbf{N}_6 = \begin{bmatrix} 0 & 0 & 0 & 0 \\ 0 & 0 & 0 & 0 \\ 0 & 0 & 0 & 0 \\ 0 & 0 & 0 & -\lambda_{10} \end{bmatrix}, \mathbf{N}_7 = \begin{bmatrix} 0 & 0 & 0 & 0 \\ 0 & 0 & 0 & 0 \\ 0 & 0 & 0 & 0 \\ 0 & 0 & 0 & -\lambda_{12} \end{bmatrix}, \mathbf{N}_8 = \begin{bmatrix} 0 & 0 & 0 & 0 \\ 0 & 0 & 0 & 0 \\ 0 & 0 & 0 & \lambda_{13} \\ 0 & 0 & 0 & 0 \end{bmatrix}.
\end{array} \right. \quad (12)$$

基于 PINNs, 我们定义 $f(x, z)$ 为

$$\begin{aligned}
f = & N_1 \mathbf{u}_1 + N_2 \mathbf{u}_2 + N_3 \mathbf{u}_3 + N_4 \mathbf{u}_4 + N_5 \mathbf{u}_5 + \\
& N_6(\mathbf{u}_6 + \mathbf{u}_8) + N_7(\mathbf{u}_7 + \mathbf{u}_9) + N_8 \mathbf{u}_{10} - \mathbf{q}.
\end{aligned} \quad (13)$$

针对本文研究问题, 损失函数定义为

$$\delta_{\text{Loss}} = L_u + L_f, \quad (14)$$

其中

$$L_u = \frac{1}{N} \sum_{i=1}^N |\mathbf{u}^{\text{pre}}(x_i, z_i) - \mathbf{u}^{\text{ref}}(x_i, z_i)|^2, \quad (15)$$

$$L_f = \frac{1}{N} \sum_{i=1}^N |f(x_i, z_i)|^2. \quad (16)$$

在上述公式中, $\mathbf{u}^{\text{pre}}(x_i, z_i)$ 和 $f(x_i, z_i)$ 分别是 PINNs 各物理量预测值和式(13)的预测值, $\mathbf{u}^{\text{ref}}(x_i, z_i)$ 是数据的真实值, N 是训练数据集的大小.图 2 为 PINNs 的训练和预测过程示意图.其具体过程为:首先,由仿真或实验获得原始数据集(包含边界条件和结果数据),经过归一化处理得到训练数据集,再将训练数据集输入到全链接神经网络模型中,并通过式(13)进行物理信息约束.然后,通过使用 L-BFGS 优化器对均方误差损失函数进行学习.当均方误差损失函数值 δ_{Loss} 最小化时,我们可以认为模型已经训练好,从而得到参数 λ 的数值,再将 λ 代入物理信息神经网络中对要求的物理量进行预测分析.

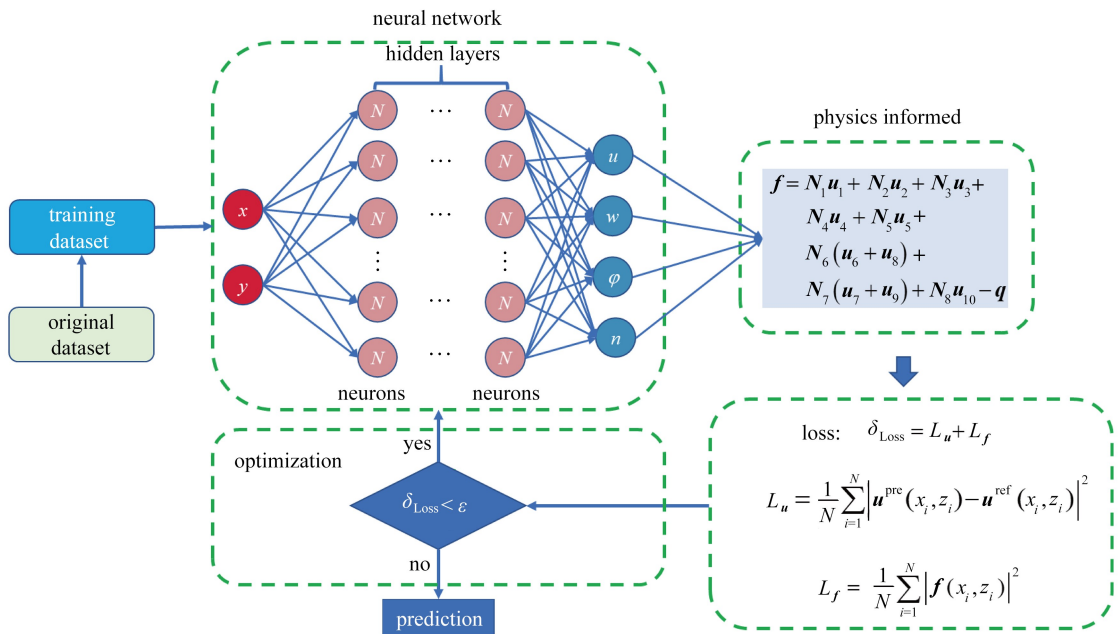


图 2 PINNs 的训练和预测过程

Fig. 2 The training and prediction process of PINNs

注 为了解释图中的颜色,读者可以参考本文的电子网页版本,后同.

图 2 中,原始数据集可通过 COMSOL 非线性模型获得,经过归一化处理得到训练数据集,归一化公式为

$$x_{\text{norm}} = \frac{x - x_{\min}}{x_{\max} - x_{\min}},$$

其中 x , x_{\max} 和 x_{\min} 分别为原始数据、原始数据的最大值和原始数据的最小值.

3 数值分析

本节中,我们将利用所构建的针对压电半导体梁结构的 PINNs 模型,计算如图 3 所示的 n 型 ZnO 压电半导体梁在静态均布载荷作用下的多场耦合力学响应.作为算例,假设压电半导体梁的长为 $10 \mu\text{m}$ 、高为 $2 \mu\text{m}$,初始载流子浓度 $n_0 = 10^{21} \text{ m}^{-3}$.考虑电子器件中常用的梁,即一端固支另一端自由(CF)和两端固支(CC).图 3(a)为一端固支另一端自由情况的悬臂梁,其上表面受 $F = 0.05 \text{ N}/\mu\text{m}$ 垂直向下的均布载荷,力学边界条件为 $u(0, z) = w(0, z) = 0$ 以及右端的轴力与剪力都为零.图 3(b)是两端均固支的梁,其上表面受 $F = 0.10 \text{ N}/\mu\text{m}$ 垂直向下的均布载荷,力学边界条件为 $u(0, z) = u(10^{-5}, z) = w(0, z) = w(10^{-5}, z) = 0$.对于图 3 所

示两种情况的梁,它们两端的电学边界条件为电学开路和电学绝缘条件,即 $D_x(0, z) = D_x(10^{-5}, z) = J_x(0, z) = J_x(10^{-5}, z) = 0$. ZnO 的材料参数取之于文献[37].在本文算例中所采用的 PINNs 模型的具体方案为:隐藏层、神经元数量和训练次数分别被设定为 5 层、50 个和 50 000 次,选用 tanh 函数作为激活函数,对于训练数据集我们采用 COMSOL 的仿真结果,也就是在其计算结果中随机选取 2 000 个样本点作为训练数据集,后续所有的算例均采用此方案.

为了验证本文所构建的 PINNs 模型求解非线性多场耦合力学问题的正确性,我们将 PINNs 模型获得的预测结果与 COMSOL 的计算结果进行比较,如表 1 和图 4 所示.表 1 给出了 COMSOL 和 PINNs 得到的位移、电势和电子浓度的最大值,可以看出, PINNs 预测结果与 COMSOL 结果吻合较好.图 4 给出了位移、电势以及电子浓度的云图分布,从图中可以看出 PINNs 预测的位移结果分布与 COMSOL 结果吻合较好,在电势和电子浓度分布上有微小差别,这是由训练集的大小所造成的.从表 1 和图 4 中可以看出, PINNs 预测的结果与 COMSOL 结果吻合较好, PINNs 可以很好地用于分析压电半导体梁多场耦合问题.

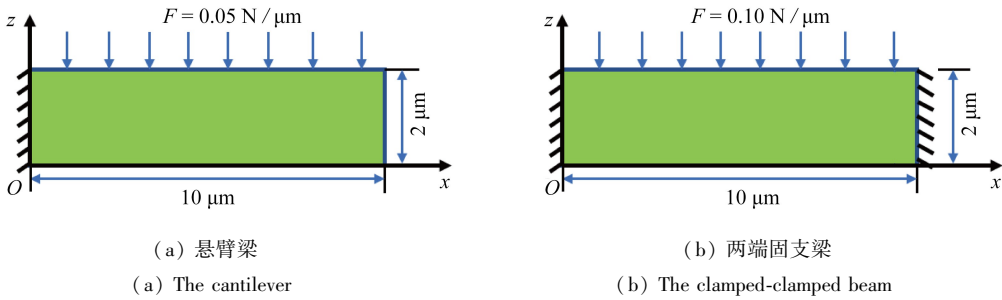


图 3 压电半导体梁示意图

Fig. 3 The sketch of PS beams

表 1 压电半导体悬臂梁的位移、电势和电子浓度最大值

Table 1 Maximum displacements, electric potentials and electron concentrations of the PS cantilever

	displacement $u / (10^{-11} \cdot \text{m})$	displacement $w / (10^{-10} \cdot \text{m})$	electric potential φ / V	electron concentration $n / (10^{21} \cdot \text{m}^3)$
COMSOL	-8.430 0	-6.690 0	-1.237 1	1.200 0
PINNs	-8.864 2	-6.715 2	-1.234 5	1.198 1
relative error $\bar{\varepsilon} / \%$	5.15	0.36	0.21	0.15

接下来,考虑图 3(b)两端固支的情况.采用同样的方法,我们将 PINNs 模型获得的预测结果与 COMSOL 的计算结果进行了比较,表 2 和图 5 分别给出了位移、电势和电子浓度的最大值及其分布云图.从表 2 和图 5 中可以看出, PINNs 模型的预测结果与 COMSOL 结果吻合得较好.从表 1 和表 2 以及图 4 和图 5 中可以看出, PINNs 能很好地分析不同工况下的压电半导体梁多场耦合力学响应.由图 4 和图 5 可知,悬臂梁情况下的电势和电子浓度的峰值点在自由端,而两端固支梁的电势和电子浓度峰值点在梁的中间截面处.

表 2 两端固支压电半导体梁的位移、电势和电子浓度最大值

Table 2 Maximum displacements, electric potentials and electron concentrations of the PS beam with CC boundary conditions

	displacement $u / (10^{-12} \cdot \text{m})$	displacement $w / (10^{-11} \cdot \text{m})$	electric potential φ / V	electron concentration $n / (10^{21} \cdot \text{m}^3)$
COMSOL	-8.540 0	-4.310 0	0.055 1	1.260 0
PINNs	-8.419 6	-4.286 3	0.055 4	1.232 4
relative error $\bar{\varepsilon} / \%$	1.41	0.55	0.54	2.19

接下来,我们在所构建的适用于压电半导体变形-极化-载流子多场耦合问题 PINNs 的基础上,通过删除或略去相应的物理量,可依次退化到压电和纯弹性梁的情况.首先,将其退化到压电梁,通过在式(13)中删除电子浓度变量,即可得到针对压电梁情况的学习函数.针对如图 3(a)所示的压电悬臂梁,其结构尺寸和所用到的材料常数均与上述压电半导体悬臂梁例子中的相同,利用退化得到的 PINNs 模型即可计算压电悬臂梁在均布载荷作用下的多场耦合力学响应.表 3 给出了由 PINNs 模型和 COMSOL 计算得到的最大位移和最大

电势,图 6 给出了由 COMSOL 和 PINNs 模型计算得到的位移和电势分布.从表 3 和图 6 中均可看出,采用本文构建的 PINNs 模型和 COMSOL 计算得到的两种结果吻合得较好.进一步可知,本文所构建的 PINNs 模型的预测结果是正确的.此外,通过比较图 4 和图 6 中由两种方法得到的电势云图可知,所构建的 PINNs 模型在求解压电结构的多场耦合响应时,相对于求解压电半导体结构来说,具有较高的精度.

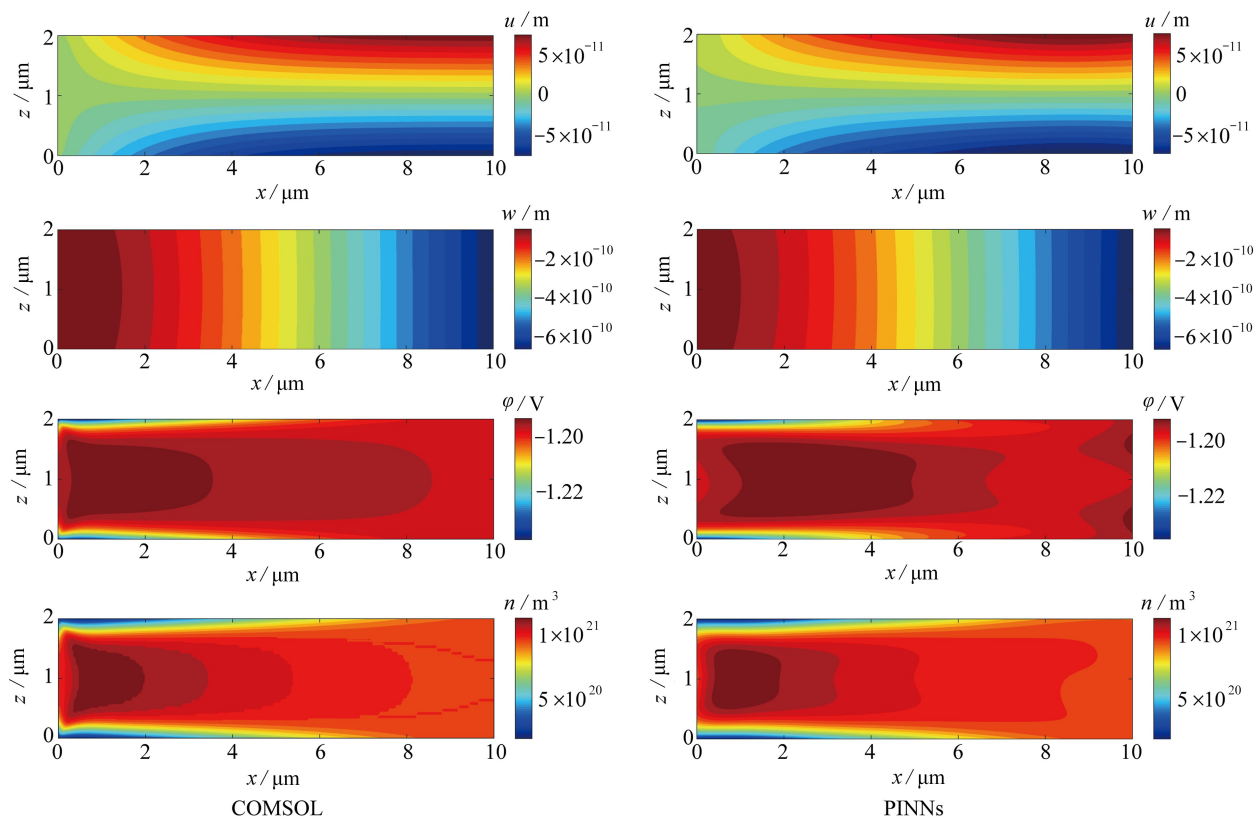


图 4 压电半导体悬臂梁的位移、电势和电子浓度分布

Fig. 4 Distributions of displacements, electric potentials and electron concentrations of the PS cantilever

表 3 压电悬臂梁的位移和电势最大值

Table 3 Maximum displacements and electric potentials of the piezoelectric cantilever

	displacement $u / (10^{-11} \cdot \text{m})$	displacement $w / (10^{-10} \cdot \text{m})$	electric potential φ / V
COMSOL	-7.940 0	-6.310 0	-0.164 8
PINNs	-7.949 8	-6.301 3	-0.165 5
relative error $\bar{\varepsilon} / \%$	0.12	0.14	0.42

为了进一步验证本文所构建的 PINNs 模型在求解非线性偏微分方程时的有效性和精确性,通过在式 (13) 中删除电势和电子浓度变量,将其退化到纯弹性梁的情况,并采用退化的 PINNs 模型计算弹性梁结构在均布载荷作用下的多场耦合力学响应.同样,计算中采用的结构尺寸和弹性材料常数均与上述压电半导体以及压电悬臂梁例子中的一样.表 4 给出了由 PINNs 模型和 COMSOL 两种方法计算得到的最大位移,可以看出, PINNs 模型的结果与 COMSOL 的结果相比,误差不超过千分之一.

表 4 纯弹性悬臂梁的位移最大值

Table 4 Maximum displacements of the pure elastic cantilever

	displacement $u / (10^{-11} \cdot \text{m})$	displacement $w / (10^{-10} \cdot \text{m})$
COMSOL	-8.840 0	-7.000 8
PINNs	-8.832 0	-7.000 6
relative error $\bar{\varepsilon} / \%$	0.090	0.002

图7给出了由两种方法计算得到的位移分布,可见二者吻合得很好.此外,通过与压电悬臂梁情况的最大位移(见表3)和位移分布(见图6)相比,所构建的PINNs模型对纯弹性梁时的预测结果精度要大于对压电梁的.通过比较所构建的PINNs模型对三种材料的梁的预测结果可知:随着所研究对象的控制方程的未知物理量的减少(也可以称为“系统复杂度的减小”),所构建的PINNs模型的求解精度会进一步提高.

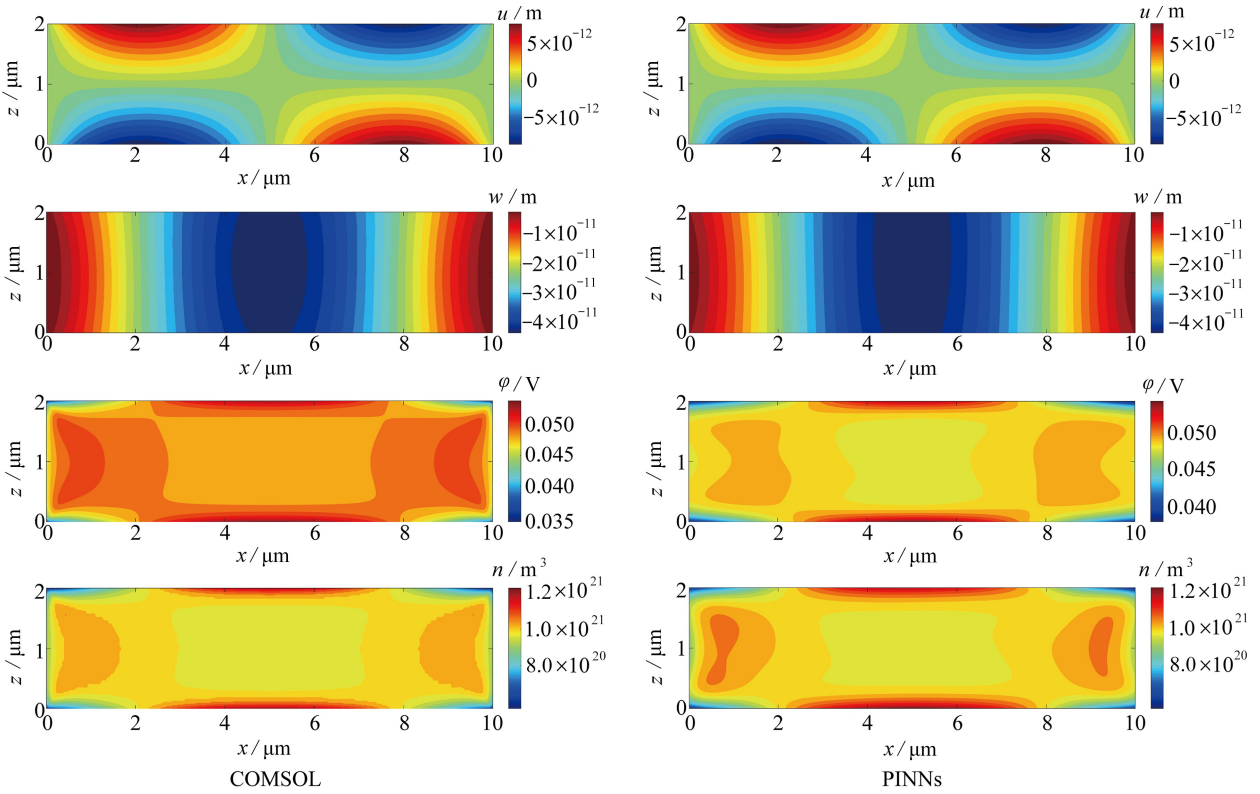


图5 两端固支压电半导体梁的位移、电势和电子浓度分布

Fig. 5 Distributions of displacements, electric potentials and electron concentrations of the PS beam with CC boundary conditions

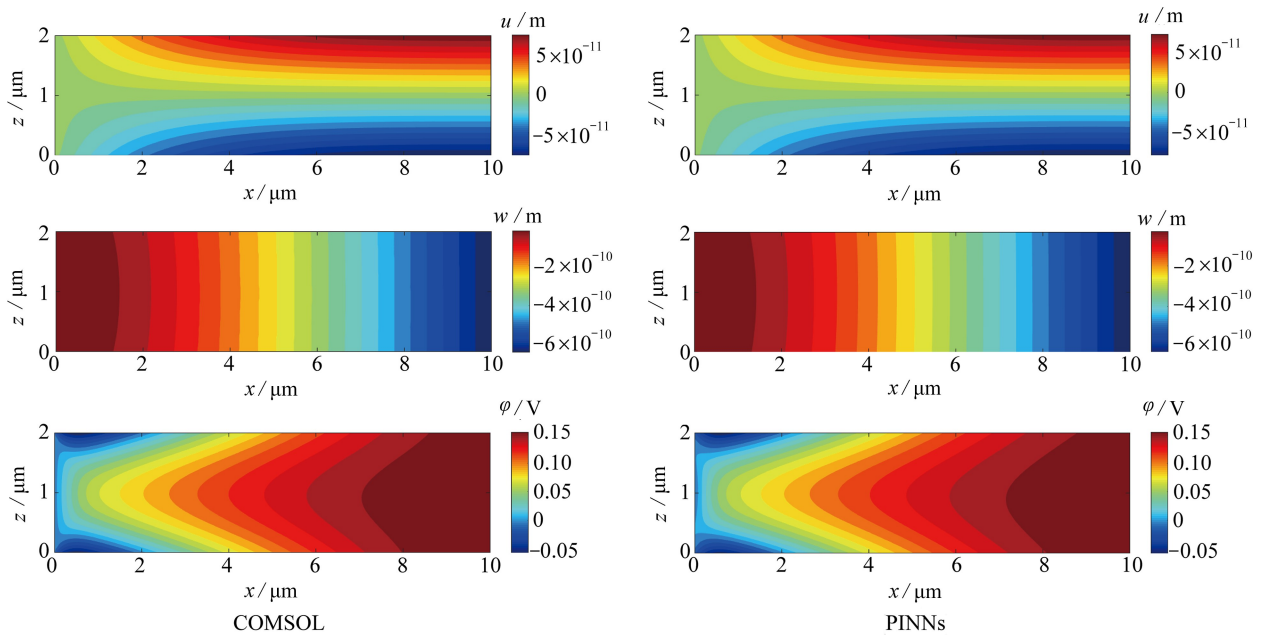


图6 压电悬臂梁位移和电势分布

Fig. 6 Distributions of displacements and electric potentials of the piezoelectric cantilever

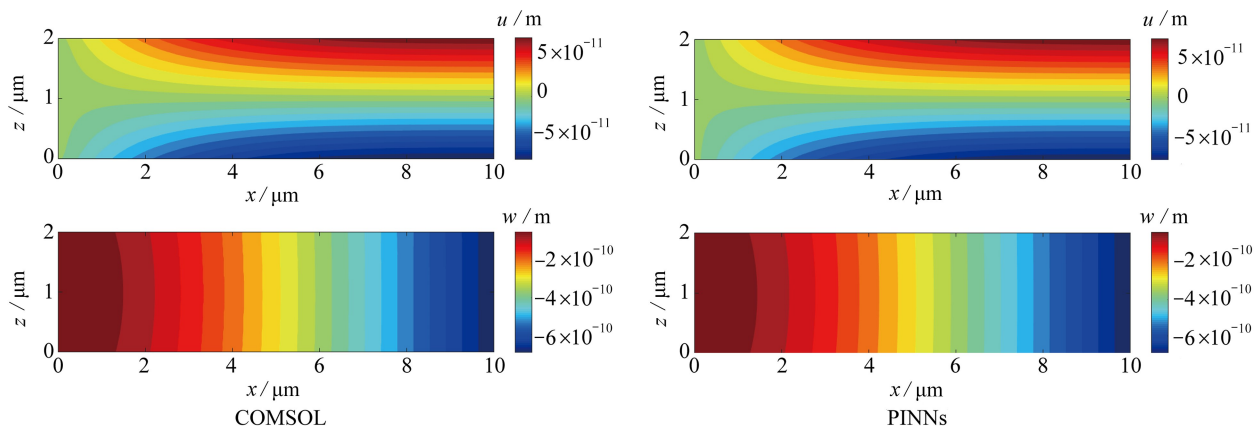


图 7 纯弹性悬臂梁的位移分布

Fig. 7 Distributions of displacements of the pure elastic cantilever

4 结 论

本文把压电半导体的控制方程嵌入到 PINNs 模型中,提出了基于 PINNs 模型的压电半导体梁非线性多场耦合力学响应的高效高精预测方法,并验证了其有效性和精确性.进一步地,通过在学习函数中删除相应的物理量,把所构建的 PINNs 模型退化到压电梁和弹性梁的情况.针对梁的两种边界约束情况(即悬臂梁和两端固支梁),采用所构建的 PINNs 模型分别研究了压电半导体梁、压电梁和纯弹性梁在均布荷载作用下的力学响应.数值结果表明:本文所提出的 PINNs 模型在压电半导体梁、压电梁和弹性梁的力学行为预测方面均有较高的精度;随着所研究对象物理量的减少,其预测结果精确度会增加.综合来说,本文所构建的 PINNs 模型为研究和预测压电半导体(以及压电和弹性)结构的非线性多场耦合力学响应提供了一个有效的工具,将有助于压电半导体(和压电)器件的研发与应用.

致谢 本文作者衷心感谢浣江实验室专项项目对本文的资助.

参考文献(References):

- [1] HICKERNELL F S. The piezoelectric semiconductor and acoustoelectronic device development in the sixties [J]. *IEEE Transactions on Ultrasonics, Ferroelectrics, and Frequency Control*, 2005, **52**(5): 737-745.
- [2] QIN Y, WANG X D, WANG Z L. Microfibre-nanowire hybrid structure for energy scavenging[J]. *Nature*, 2008, **451**(7180): 809-813.
- [3] LIU Y, YANG Q, ZHANG Y, et al. Nanowire piezo-phototronic photodetector: theory and experimental design [J]. *Advanced Materials*, 2012, **24**(11): 1410-1417.
- [4] HAN W H, ZHOU Y S, ZHANG Y, et al. Strain-gated piezotronic transistors based on vertical zinc oxide nanowires[J]. *ACS Nano*, 2012, **6**(5): 3760-3766.
- [5] WANG Z L. Piezopotential gated nanowire devices: piezotronics and piezo-phototronics[J]. *Nano Today*, 2010, **5**(6): 540-552.
- [6] 罗逸琛. 层状压电半导体结构的多场耦合力学行为分析[D]. 杭州: 浙江大学, 2019. (LUO Yixun. Analysis of multi-field coupling mechanical behavior of laminated piezoelectric semiconductor structures[D]. Hangzhou: Zhejiang University, 2019. (in Chinese))
- [7] 梁超, 张春利. 恒磁场作用下压磁/压电半导体复合圆柱壳的耦合响应分析[J]. *固体力学学报*, 2020, **41**(3): 206-215. (LIANG Chao, ZHANG Chunli. Analysis of multi-field coupling responses of piezomagnetic/piezoelectric semiconductor cylindrical shell under a constant magnetic field[J]. *Chinese Journal of Solid Mechanics*, 2020, **41**(3): 206-215. (in Chinese))
- [8] 程若然, 张春利. 多个局部温度载荷下压电半导体纤维杆的压电电子学行为分析[J]. *力学学报*, 2020, **52**(5):

- 1295-1303. (CHENG Ruoran, ZHANG Chunli. Analysis of the piezotronic effect of a piezoelectric semiconductor fiber under multiple local temperature loadings[J]. *Chinese Journal of Theoretical and Applied Mechanics*, 2020, **52**(5): 1295-1303. (in Chinese))
- [9] 李德志, 张春利. 弹性纵波在压电-压电半导体周期杆中的传播[J]. 哈尔滨工程大学学报, 2022, **43**(9): 1252-1257. (LI Dezhi, ZHANG Chunli. Propagation of elastic longitudinal waves in a periodic piezoelectric-piezosemiconductor rod[J]. *Journal of Harbin Engineering University*, 2022, **43**(9): 1252-1257. (in Chinese))
- [10] ZHANG C L, WANG X Y, CHEN W Q, et al. Carrier distribution and electromechanical fields in a free piezoelectric semiconductor rod[J]. *Journal of Zhejiang University (Science A)*, 2016, **17**(1): 37-44.
- [11] 王晓媛. 一维压电半导体杆的力学行为研究[D]. 杭州: 浙江大学, 2017. (WANG Xiaoyuan. Research on mechanical behaviors of one-dimensional piezoelectric semiconductor rods[D]. Hangzhou: Zhejiang University, 2017. (in Chinese))
- [12] CHENG R R, ZHANG C L, CHEN W Q, et al. Temperature effects on mobile charges in extension of composite fibers of piezoelectric dielectrics and non-piezoelectric semiconductors[J]. *International Journal of Applied Mechanics*, 2019, **11**(9): 1950088.
- [13] LUO Y X, ZHANG C L, CHEN W Q, et al. Thermally induced electromechanical fields in unimorphs of piezoelectric dielectrics and nonpiezoelectric semiconductors[J]. *Integrated Ferroelectrics*, 2020, **211**(1): 117-131.
- [14] ZHANG C L, WANG X Y, CHEN W Q, et al. An analysis of the extension of a ZnO piezoelectric semiconductor nanofiber under an axial force[J]. *Smart Materials and Structures*, 2017, **26**(2): 025030.
- [15] FAN S Q, HU Y T, YANG J S. Stress-induced potential barriers and charge distributions in a piezoelectric semiconductor nanofiber[J]. *Applied Mathematics and Mechanics (English Edition)*, 2019, **40**(5): 591-600.
- [16] HUANG H Y, QIAN Z H, YANG J S. I-V characteristics of a piezoelectric semiconductor nanofiber under local tensile/compressive stress[J]. *Journal of Applied Physics*, 2019, **126**(16): 164902.
- [17] ANCONA M G, BINARI S C, MEYER D J. Fully coupled thermoelectromechanical analysis of GaN high electron mobility transistor degradation[J]. *Journal of Applied Physics*, 2012, **111**(7): 074504.
- [18] ANCONA M G. Fully coupled thermoelectroelastic simulations of GaN devices[C]//2012 International Electron Devices Meeting. San Francisco, CA, USA, 2012: 13.5.1-13.5.4.
- [19] ANCONA M G. Nonlinear thermoelectroelastic simulation of III-N devices[C]//2014 International Conference on Simulation of Semiconductor Processes and Devices (SISPAD). Yokohama, Japan, 2014: 121-124.
- [20] ANCONA M G. Nonlinear thermoelectroelastic analysis of III-N semiconductor devices[J]. *IEEE Journal of the Electron Devices Society*, 2017, **5**(5): 320-334.
- [21] ZHAO M H, ZHANG Q Y, FAN C. An efficient iteration approach for nonlinear boundary value problems in 2D piezoelectric semiconductors[J]. *Applied Mathematical Modelling*, 2019, **74**: 170-183.
- [22] ZHAO M H, MA Z L, LU C S, et al. Application of the homotopy analysis method to nonlinear characteristics of a piezoelectric semiconductor fiber[J]. *Applied Mathematics and Mechanics (English Edition)*, 2021, **42**(5): 665-676.
- [23] ZHAO M H, YANG C H, FAN C Y, et al. A shooting method for nonlinear boundary value problems in a thermal piezoelectric semiconductor plate[J]. *ZAMM Journal of Applied Mathematics and Mechanics*, 2020, **100**(12): e201900302.
- [24] BAO G F, LI D Z, KONG D J, et al. Analysis of axially loaded piezoelectric semiconductor rods with geometric nonlinearity[J]. *International Journal of Applied Mechanics*, 2022, **14**(10): 2250104.
- [25] PANG G, D'ELIA M, PARKS M, et al. nPINNs: nonlocal physics-informed neural networks for a parametrized nonlocal universal Laplacian operator. Algorithms and applications[J]. *Journal of Computational Physics*, 2020, **422**: 109760.
- [26] HAGHIGHAT E, JUANES R. SciANN: a Keras/TensorFlow wrapper for scientific computations and physics-informed deep learning using artificial neural networks[J]. *Computer Methods in Applied Mechanics and Engineering*, 2021, **373**: 113552.

- [27] MENG X, LI Z, ZHANG D, et al. PPINN: parareal physics-informed neural network for time-dependent PDEs [J]. *Computer Methods in Applied Mechanics and Engineering*, 2020, **370**: 113250.
- [28] ZHAO Q K, YANG H Y, LIU J B, et al. Machine learning-assisted discovery of strong and conductive Cu alloys: data mining from discarded experiments and physical features [J]. *Materials & Design*, 2021, **197**: 109248.
- [29] LIU X, ATHANASIOU C E, PADTURE N P, et al. A machine learning approach to fracture mechanics problems [J]. *Acta Materialia*, 2020, **190**: 105-112.
- [30] HENKES A, WESSELS H, MAHNKEN R. Physics informed neural networks for continuum micromechanics [J]. *Computer Methods in Applied Mechanics and Engineering*, 2022, **393**: 114790.
- [31] ATHREYA A P, BRÜCKL T, BINDER E B, et al. Prediction of short-term antidepressant response using probabilistic graphical models with replication across multiple drugs and treatment settings [J]. *Neuropsychopharmacology*, 2021, **46**(7): 1272-1282.
- [32] RAISSI M, PERDIKARIS P, KARNIADAKIS G E. Physics-informed neural networks: a deep learning framework for solving forward and inverse problems involving nonlinear partial differential equations [J]. *Journal of Computational Physics*, 2019, **378**: 686-707.
- [33] JAGTAP A D, KARNIADAKIS G E. Extended physics-informed neural networks (XPINNs): a generalized space-time domain decomposition based deep learning framework for nonlinear partial differential equations [J]. *Communications in Computational Physics*, 2020, **28**(5): 2002-2041.
- [34] RAISSI M, YAZDANI A, KARNIADAKIS G E. Hidden fluid mechanics: learning velocity and pressure fields from flow visualizations [J]. *Science*, 2020, **367**(6481): 1026-1030.
- [35] HAGHIGHAT E, RAISSI M, MOURE A, et al. A physics-informed deep learning framework for inversion and surrogate modeling in solid mechanics [J]. *Computer Methods in Applied Mechanics and Engineering*, 2021, **379**: 113741.
- [36] REDDY J N. *Mechanics of Laminated Composite Plates and Shells* [M]. CRC Press, 2004.
- [37] AULD B A. *Acoustic Fields and Waves in Solids* [M]. Vol 1. Wiley-Inter Science Publication, 1974.